Journal of Drug Delivery Science and Technology 109 (2025) 106974

Contents lists available at ScienceDirect

Journal of Drug Delivery Science and Technology

journal homepage: www.elsevier.com/locate/jddst

Higher-order multicomponent crystals as a strategy to decrease the IC_{50} parameter: the case of praziquantel, niclosamide and acetic acid

Ilenia D'Abbrunzo [a], Lara Gigli [b], Nicola Demitri [b], Chiara Sabena [c], Carlo Nervi [c,d], Michele R. Chierotti [c], Serena Bertoni [e], Irena Škorić [f], Cécile Häberli [g,h], Jennifer Keiser [g,h], Dritan Hasa [a,*], Beatrice Perissutti [a,**]

[a] Department of Chemical and Pharmaceutical Sciences, University of Trieste, P.le Europa 1, 34127, Trieste, Italy
[b] Elettra-Sincrotrone Trieste, S.S. 14 Km 163.5 in Area Science Park, Basovizza, Trieste, Italy
[c] Department of Chemistry and NIS Centre, University of Torino, V. Giuria 7, 10125, Torino, Italy
[d] Skolkovo Institute of Science and Technology, Bolshoy Boulevard 30, bldg. 1, Moscow, 121205, Russia
[e] Department of Pharmacy and Biotechnology, University of Bologna, V. S. Donato 19/2, 40127, Bologna, Italy
[f] Department of Organic Chemistry, Faculty of Chemical Engineering and Technology, University of Zagreb, Marulićev trg 19, 10000, Zagreb, Croatia
[g] Department of Medical Parasitology, Swiss Tropical and Public Health Institute, 4123, Allschwil, Switzerland
[h] University of Basel, Basel, 4000, Switzerland

ARTICLE INFO

Keywords:
Praziquantel-niclosamide-acetic acid cocrystal solvate
Pharmaceutically acceptable cocrystal solvate
Synchrotron X-ray powder diffraction
Building-blocks approach
In vitro anthelmintic activity
In vivo preliminary tests

ABSTRACT

We successfully assembled via mechanochemistry 3 anthelmintic molecules in a single stable solid, namely praziquantel (PZQ), niclosamide (NCM), and acetic acid (AA). We obtained a cocrystal solvate with largely superior anthelmintic activity against *in vitro* Schistosoma *mansoni* adults and, notably, against Newly Transformed Schistosomula compared to pure individual drugs (i.e., PZQ and NCM) and to its binary counterparts (i.e., PZQ-NCM cocrystal and PZQ-AA monosolvate).

We also demonstrated 5 different strategies for synthesizing the ternary cocrystal not only starting from individual coformers but also by combining different building blocks (i.e. preformed binary solids). The new phase was only obtainable through mechanochemistry as comparative slurry experiments were unsuccessful. Even though the ternary solid was crystallized through all five investigated routes, a pure phase was obtained by milling the preformed praziquantel-acetic acid monosolvate and raw niclosamide in an equimolar ratio for 60 min in the presence of 160 μL of acetic acid. Acetic acid acted both as a solvate-forming molecule and a liquid additive.

The purity of this new solid phase was confirmed by SS-NMR spectrum, also suggesting the presence of one independent molecule of PZQ, one of NCM and one of AA, as confirmed by ^{1}H NMR. The cocrystal structure was solved from the Synchrotron powder X-ray pattern and optimized via DFT calculations. Crystallizing in the triclinic *P*-1 space group, the solid comprises one PZQ, one NCM, and one AA molecule linked via hydrogen bonds, as demonstrated by FT-IR analyses. The solid phase exhibits small plate agglomerates, as observed through SEM analysis, a desolvation event at ~107 °C (TGA weight loss: 9.77 %), and physical stability over 24 months at room temperature.

The drastic reduction in IC50 (0.01 μM against Newly Transformed Schistosomula and Schistosoma *mansoni* adults) of the new solid fully justifies the ambitious challenge of incorporating more than two components into a single crystalline phase, underscoring the pivotal role of the ternary system in enhancing bioactivity. This finding highlights the need to tackle the next challenge: identifying the most suitable oral dosage form for a cocrystal solvate, a requirement that remains unmet in the pilot studies conducted in this work.

Abbreviations: APIs, active pharmaceutical ingredients; PZQ, praziquantel; NCM, niclosamide; AA, acetic acid; DSC, differential scanning calorimetry; PXRD, Powder X-ray diffraction; LAG, liquid-assisted grinding; NG, neat grinding; FT-IR, infrared spectroscopy; SSNMR, solid-state NMR; DFT, Density Functional Theory; SEM, scanning electron microscopy; CSD, Cambridge Structural Database; NTS, Newly Transformed Schistosomula; S. *mansoni*, adult Schistosoma *mansoni*; WBR, worm burden reduction; TMS, tetramethyl silane; ASU, asymmetric unit; RH, relative humidity.

* Corresponding author.
** Corresponding author.
E-mail addresses: dhasa@units.it (D. Hasa), bperissutti@units.it (B. Perissutti).

https://doi.org/10.1016/j.jddst.2025.106974
Received 17 February 2025; Received in revised form 15 April 2025; Accepted 25 April 2025
Available online 25 April 2025

1. Introduction

Solvated crystals are multicomponent solids that contain molecules of one (or more) solvent/s incorporated into their crystal lattice [1]. As a result, a solvated solid often (an exception is given by the of isostructural solvates [2]) exhibits a different crystal structure than its anhydrous form, consequently also different physicochemical properties, including solubility, dissolution (eventually bioavailability) and both physical and chemical stability. Contrary to hydrates (i.e. solvates containing water in their crystalline structure [1]), solvates are infrequently used in pharmaceutical products, primarily due to potential toxicity issues as regulated by the ICH guideline Q3C on residual solvents in pharmaceuticals [3].

In fact, to the best of our knowledge, only few pharmaceuticals are marketed as solvates (i.e., trametinib [4], dapagliflozin [5], cabazitaxel [6], darunavir [7], doxycycline [8], indinavir sulfate [9] and warfarin sodium [10]), with three of them dosed as ethanolates.

In 2021, Werner and Swift published a study listing the 50 most present solvate classes in the Cambridge Structural Database (CSD) [11], where acetic acid (AA) solvates occupy the 17th position with 341 cases reported (1.08 % of the total). Among them, temozolomide-AA solvate monohydrate [12], temozolomide-AA solvate [12], phenarsazine chloride-AA solvate [13], cephaloglycine-AA solvate monohydrate [14], praziquantel-AA solvate [15], sertraline hydrochloride-AA solvate [16], galunisertib-AA solvate [17] are just some of the solvated APIs containing AA reported in the CSD. In this study, we report a new three-components solvate containing AA, praziquantel (PZQ) and niclosamide (NCM) (PZQ-NCM-AA, Fig. 1), all having demonstrated anthelmintic properties. Indeed, PZQ is a first-choice drug for the treatment of schistosomiasis, that is an infection caused by trematodes of the genus *Schistosoma* [18]. NCM is mainly applied to cure parasite infestations, such as those of tapeworms and cestode [19]. AA has recently shown anthelmintic activity (against *Gyrodactylus Kobayashii* trematode) in fish [20], although its efficacy against schistosomes remains to be demonstrated. While its oral administration in humans is obviously not feasible, its incorporation into a cocrystal could enable its use as an anthelmintic.

As far as we know, literature does not provide examples of cocrystal solvates where all three components – two solids and one liquid – are active molecules with the same therapeutic activity (in this case, all being anthelmintic). Combining three different molecules having the same therapeutic activity can bring to additional advantages, including the synergistic effect, potentially allowing for a simplification of the individual drug dosage, and reducing drug resistance [21,22]. Noteworthy, the simultaneous administration of three different molecules in the form of a cocrystal can possibly bring to an increase of the potency of a drug, for example, by reducing the half-maximal inhibitory concentration (IC50), compared to the values of each molecules considered singularly, in absence of any covalent modification of the drug. This was also the objective of the present study.

PZQ-NCM-AA can be considered as a pharmaceutically acceptable solvate since AA is classified as a GRAS substance [23], being frequently used in the food industry as an antimicrobial agent, flavor enhancer, flavoring agent, adjuvant and pH control agent [24]. Furthermore, in accordance with ICH guideline Q3C, which sets limits on residual solvents in pharmaceutical products, AA is classified as a class 3 solvent, indicating low toxicity and minimal risk to human health [3].

In our previous study [25], which resulted in a binary antiparasitic cocrystal of PZQ and NCM (CSD refcode RIPFOP01), we observed the formation of a drug-drug binary cocrystal, which we are aiming to transform into a ternary cocrystal solvate with AA. For this purpose, five different synthetic strategies (which will be detailed in this work) were investigated using mechanochemistry, with the idea of starting with five distinct building blocks and adding the "missing piece" for each strategy to get the same cocrystal solvate. We successfully obtained the same cocrystal solvate through all the explored mechanochemical routes, though with varying yields. Slurry experiments, conducted for comparative purposes, did not result in the formation of the cocrystal solvate at any point. This highlights the significant potential of solid-state techniques like mechanochemistry in efficiently and effectively achieving the desired outcome.

Among different mechanochemical routes, PZQ-NCM-AA cocrystal solvate was obtained as a pure phase by grinding preformed PZQ-AA monosolvate and raw NCM in an equimolar ratio, with the addition of micromolar amounts of AA (i.e., 160 μL). The structure of the cocrystal solvate was successfully solved and refined from the Synchrotron PXRD data and its geometry was optimized by DFT calculations. To characterize the cocrystal solvate, a combination of techniques was employed, including differential scanning calorimetry (DSC), thermogravimetric analysis (TGA), infrared spectroscopy (FT-IR), solid-state NMR (SSNMR), ^{1}H NMR and scanning electron microscopy (SEM). Investigations also comprised assessing the chemical and physical stability under various conditions (i.e., drug recovery, physical stability as solid phase and under high relative humidity (RH)).

Finally, *in vitro* anthelminthic activity against Newly Transformed Schistosomula (NTS), and adult Schistosoma *mansoni* (S. *mansoni*) of the single components, the known binary systems and new ternary system was evaluated and *in vivo* preliminary tests on mice were also performed through the administration of an oily suspension of the novel phase.

2. Materials and methods

2.1. Materials

PZQ, (RS)-2-(Cyclohexylcarbonyl)-1,2,3,6,7,11b-hexahydro-4-H-pyrazino[2,1-a]-isoquinolin-4-one], of Ph. Eur. grade was kindly donated by Fatro S.p.a. (Bologna, Italy), while NCM (5-chloro-N-(2-chloro-4-nitrophenyl)-2-hydroxybenzamide) was purchased from Sigma-Aldrich (St. Louis, USA) with a declared purity of 98–100 %. Acetic acid (AA) was provided from Carlo Erba (Rodano-Milan, Italy).

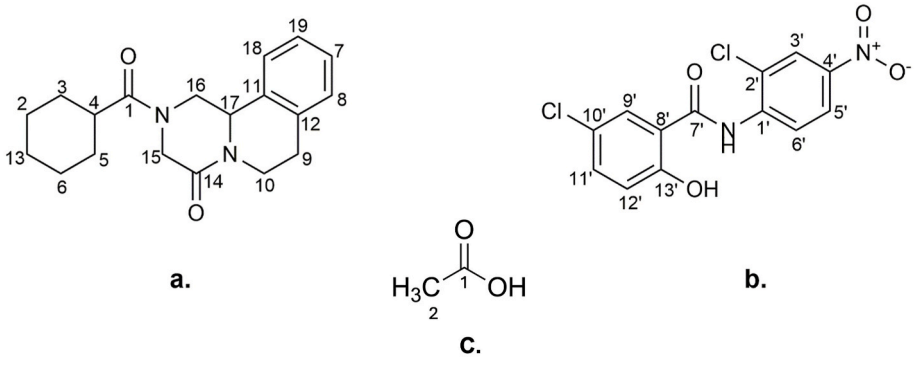

Fig. 1. (a) PZQ and (b) NCM and (c) AA molecular structures with atom numbering.

All the actives and chemicals were used without further purification.

2.2. Methods

2.2.1. Synthetic strategies for preparing PZQ-NCM-AA cocrystal solvate

2.2.1.1. Mechanochemical routes. The mechanochemical synthesis of the ternary cocrystal solvate was performed in Retsch MM400 vibrational mill (Retsch, Germany) equipped by two 25 mL stainless steel jars and one 10 mm Ø bead, respectively. Both screw cap and plug-in jars were used, with no significant differences observed in the yield of the experiments.

Five different synthetic strategies were explored to obtain the cocrystal solvate. The milling frequency for each pathway was maintained at 25 Hz, and the void volume in the jar was also kept constant (i.e., a total of about 400 mg of powder per 25 mL jar).

Each synthetic strategy was tested with three different milling times: 30, 60 and 120 min.

After a set of preliminary trials, the volume of AA added to each experiment was 160 μL (η [26] = 0.4).

2.2.1.1.1. From individual coformers. An equimolar ratio of commercial PZQ Form A and NCM Form A (i.e., 0.625 mmol which equals to 195.4 mg and 204.6 mg, respectively) was ground with 160 μL of AA. This strategy is depicted in red in Fig. 2.

2.2.1.1.2. From preformed PZQ-NCM 1:3 anhydrous cocrystal, raw PZQ and AA. Preformed PZQ-NCM 1:3 anhydrous cocrystal (indexed as RIPFOP01 in the CSD) in the amount of 269.74 mg, obtained according to the procedure reported in our previous work [25], was ground in the presence of 130.26 mg of raw PZQ Form A (to get PZQ-NCM equimolar ratio) and 160 μL of AA (pink strategy in Fig. 2).

2.2.1.1.3. From preformed PZQ-AA monosolvate, raw NCM and AA. Preformed PZQ-AA monosolvate (reported as DAJCEA in the CSD) (i.e., 212.97 mg), mechanochemically obtained according to Zanolla and coauthors' procedure [15], was ground with an equimolar ratio of solid NCM (i.e., 187.03 mg) in the presence of AA (black strategy in Fig. 2).

2.2.1.1.4. From preformed PZQ-NCM 1:1 coamorphous and AA. 400 mg of PZQ-NCM 1:1 coamorphous, mechanochemically obtained through 4h of neat grinding (NG) was ground in the presence of 160 μL of the liquid at 25 Hz (violet strategy in Fig. 2).

2.2.1.1.5. From individual coformers in the presence of preformed seeds of cocrystal solvate. An equimolar ratio of commercial PZQ Form A and NCM Form A (i.e., 175.86 mg and 184.14, respectively) was ground with 160 μL of AA in the presence of preformed seeds of the cocrystal solvate (i.e. 40 mg, corresponding to 10 % wt ratio) (blue strategy in Fig. 2).

2.2.1.2. Slurry bridging routes. For comparative purposes, slurry experiments (grey strategies in Fig. 2) were conducted adopting the procedure reported in a previous experimental study [27]. Specifically, 300 mg of solid and 5 mL of AA were placed into 10 mL glass vials equipped with a screw cap and sealed with parafilm. The suspensions (prepared in duplicate) were continuously stirred at room temperature (20 °C) for 7 days. Subsequently, the excess solid phases were recovered, filtered under vacuum pump through paper filters and characterized.

For obvious reasons, not all the above-mentioned mechanochemical routes are viable via slurry approach; three (out of the five) starting points were hence tested for comparison:

1. An equimolar ratio of commercial PZQ Form A and NCM Form A (i.e., 146.55 mg and 153.45 mg, respectively) in 5 mL of AA;
2. Preformed PZQ-NCM 1:1 coamorphous (300 mg) in 5 mL of AA;
3. Preformed PZQ-NCM 1:3 anhydrous cocrystal (300 mg) in 5 mL of AA.

2.2.2. Laboratory PXRD analysis

Laboratory PXRD analysis was carried out by a Bruker D2 Phaser benchtop diffractometer (Bruker, Manheim, Germany) using the Bragg-Brentano geometry, using Cu-Kα radiation (λ = 1.5418 Å) with a 300 W low-power X-ray generator (30 kV at 10 mA). All the measurements were conducted in a 2θ range of 3–40° with a step size of 0.02° and a scan speed of 0.6°/s.

Each sample was prepared by gently pressing approximately 200 mg of ground product into the cavity of a steel sample holder equipped with a cylindrical polyvinylidene fluoride (PVDF) reducer.

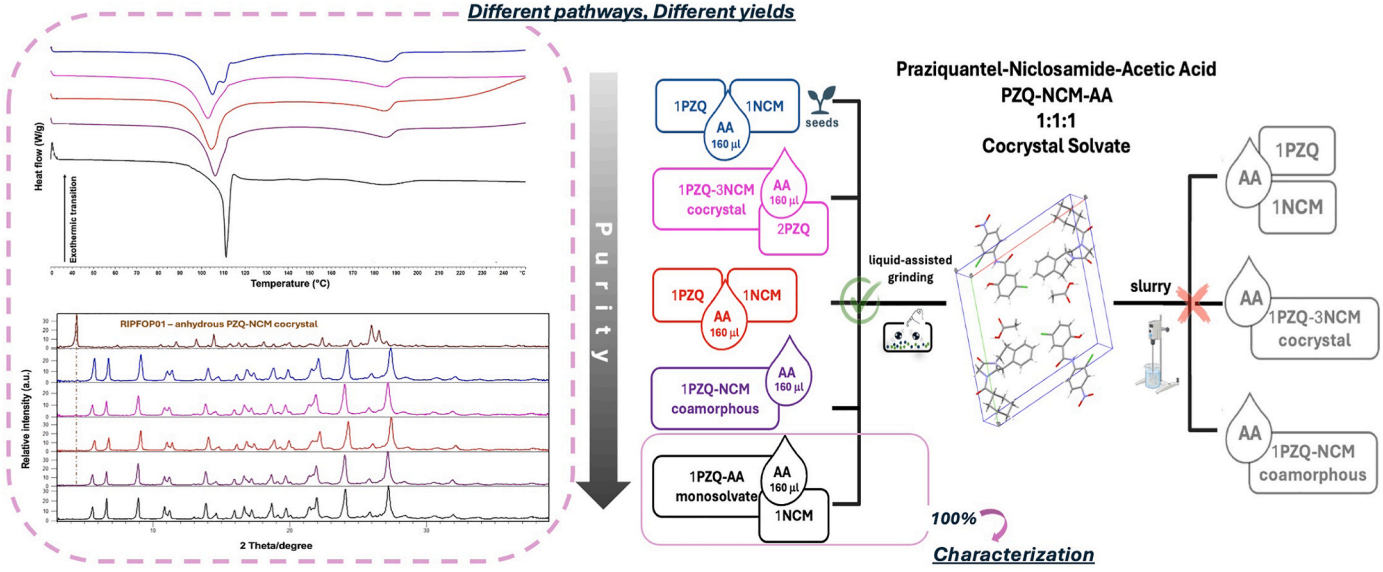

Fig. 2. Cartoon illustrating characterization results by DSC (top left) and PXRD (bottom left) of the cocrystal solvate samples obtained via different mechanochemical synthetic routes (centre). Each strategy and its corresponding DSC/PXRD data are distinguished by a specific color code: (from top to bottom) from individual coformers in the presence of preformed seeds of cocrystal solvate (blue), from preformed PZQ-NCM 1:3 anhydrous cocrystal, raw PZQ and AA (pink), from individual coformers (red), from preformed PZQ-NCM 1:1 coamorphous and AA (violet), from preformed PZQ-AA monosolvate, raw NCM and AA (black). Inefficient slurry bridging routes (grey) are depicted on the right side (their characterizations results are omitted for brevity). (For interpretation of the references to color in this figure legend, the reader is referred to the Web version of this article.)

2.2.3. Synchrotron X-ray diffraction and solution of the crystal structure

The data collection of the cocrystal obtained in powder form was performed at the X-ray diffraction beamline (XRD2) of Elettra Synchrotron (Trieste, Italy) [28]. The powder sample was measured at 298 K in transmission mode filling a boron capillary of 0.5 mm of diameter. The powder data was acquired using monochromatic wavelength of 1.00 Å on Pilatus 6M hybrid-pixel area detectors (DECTRIS Ltd., Baden-Daettwil, Switzerland). The two-dimensional powder pattern has been integrated using Fit2D program [29,30], after preliminary calibration of hardware setup, using a capillary filled with LaB_6 standard reference powder (NIST 660a).

The structure of the cocrystal form was solved through a simulated annealing (SA) protocol using EXPO2014 [31]. The starting structural model containing one PZQ molecule (TELCAQ model) [32], one molecule of NCM and one of AA and were built with Material studio software v 7.0. (MS) [33] and then geometrically optimized by the Dmol3 code implemented in MS. During the SA the cyclohexyl group of the PZQ molecule and methyl group of Acetic acid were allowed to freely rotate.

CCDC number 2391439 contains the supplementary crystallographic data for the cocrystal solvate. These data can be obtained free of charge from The Cambridge Crystallographic Data Centre via https://www.ccdc.cam.ac.uk/structures.

2.2.4. DSC analysis

For DSC analysis, each sample weighing 2–4 mg was introduced into an aluminum sealed and pierced 40 μL crucible and analyzed by a Mettler Toledo DSC 3 Star System (Milan, Italy) with a heating program of 30–250 °C (10 °C/min) under a nitrogen atmosphere (50 mL/min flow rate).

2.2.5. TGA analysis

TGA analysis was performed using a Mettler Toledo TGA TDA851 (Milan, Italy). Briefly, 3–6 mg of the powdered sample were inserted into aluminum 40 μL crucibles and analyzed with a heating program of 30–250 °C (10 °C/min) under a nitrogen atmosphere (50 mL/min flow rate).

2.2.6. FT-IR analysis

Powdered samples were analyzed with a Shimadzu IRAffinity-1S FT-IR instrument (Kyoto, Japan) in a range of 400–4000 cm^{-1} with a resolution of 4 cm^{-1} and 20 scans.

Suitable discs for analysis were prepared by gently grinding in an agate mortar 200 mg of anhydrous KBr (99 % infrared grade) with 1 % w/w of analyte and then pressing the mixture with a hydraulic press (PerkinElmer, Norwalk, USA), applying a pressure of 10 Ton for 3 min.

2.2.7. SSNMR analysis

The PZQ-NCM-AA cocrystal solvate and PZQ-AA monosolvate ^{13}C CPMAS spectra were acquired with a Jeol ECZR 600 instrument, operating at 600.17 and 150.91 MHz, respectively for ^{1}H and ^{13}C nuclei. The powder samples were packed into cylindrical zirconia rotors with a 3.2 mm o.d. and a 60 μL volume. A certain amount of sample was used without further preparation to fill the rotor. The ^{13}C CPMAS spectra were collected at room temperature at a spinning speed of 20 kHz, using a ramp cross-polarization pulse sequence with a 90° ^{1}H pulse of 2.2 μs, a contact time of 3.5 ms, an acquisition time of 29.5 ms, an optimized recycle delay of 4.2 s for PZQ-NCM-AA and 63.5 s for PZQ-AA and a number of scans between 938 and 1579. A two-pulse phase modulation (TPPM) decoupling scheme was used, with a radiofrequency field of 108.5 kHz. The ^{13}C chemical shift scale was calibrated through the methylenic signal of external standard adamantane (at 38.48 ppm with respect to tetramethyl silane, TMS).

The PZQ, NCM, PZQ-NCM 1:3 anhydrous cocrystal and PZQ-NCM 1:1 coamorphous ^{13}C CPMAS spectra were acquired with a Bruker Avance II 400 Ultra Shield instrument, operating at 400.23 and 100.63, respectively for ^{1}H and ^{13}C nuclei. Powder sample was packed into cylindrical zirconia rotors with a 4 mm o.d. and a 80 μL volume. A certain amount of sample was collected from the batch and used without further preparations to fill the rotor. ^{13}C CPMAS spectra were acquired at a spinning speed of 12 kHz, using a ramp cross-polarization pulse sequence with a 90° ^{1}H pulse of 3.60 μs, a contact time of 3 ms, optimized recycle delays between 4.4 and 40.0 s and scans numbers between 95 and 4744. For every spectrum, a two-pulse phase modulation (TPPM) decoupling scheme was used, with a radiofrequence field of 69.4 kHz. The ^{13}C chemical shift scale was calibrated through the methylenic signal of external standard glycine (at 43.7 ppm).

2.2.8. ^{1}H NMR analysis

^{1}H NMR (with deuterated chloroform, $CDCl_3$) spectra were acquired on a Jeol ECZR 600 instrument operating at 600.2 MHz. In the ^{1}H spectrum, to obtain quantitative information, it was necessary to employ a relaxation delay of 60 s. The number of scans acquired was 8.

2.2.9. DFT calculations

Solid state DFT calculations were performed with Quantum Espresso (QE, v. 6.4.1) [34], adopting the following methodology: we used the projector augmented wave (PAW) with the non-local vdW-DF2 approach [35] and the B86r functional [36], employing the SSSP set of pseudopotentials [37,38]. An energy cut-off of 60 Ry was used for geometry optimizations. NMR calculations were performed using the Gauge Including Projected Augmented Wave (GIPAW) [39] and the PBE pseudopotentials from PS Library 1.0.0 [40] with an energy cut-off of 80 Ry, following the methodology previously described [41–43]. The theoretical absolute isotropic magnetic shielding (σ_{iso}) values were converted into isotropic chemical shifts (δ_{iso}) relative to the absolute magnetic shielding of the reference substance DABCO computed at the same level, applying the following equation:

$$\delta_{iso}(calc) = \sigma_{iso}(ref) - \sigma_{iso}(calc) + \delta_{iso}(ref) \quad (1)$$

δ_{iso} (ref) ^{13}C value for DABCO has been experimentally evaluated as 47.74 ppm, while the absolute isotropic constant shielding σ_{iso} (ref) is 120.59 ppm, calculated from the reported neutron diffraction crystal structure [44].

2.2.10. SEM analysis

Images of the cocrystal solvate were collected through scanning electron microscopy (SEM). The powdered sample was placed on an aluminum stub covered with a carbon double-sided tape and sputter-coated with gold using a Sputter Coater K550X (Emitech, Quorum Technologies Ltd, UK), before being analyzed by a scanning electron microscope (Quanta 250 SEM, FEI, Oregon, USA) with the secondary electron detector. The working distance was set at 10 mm to obtain the appropriate magnifications, and the acceleration voltage was set at 5 kV.

2.2.11. Drug recovery

To check possible degradation of PZQ-NCM-AA cocrystal solvate after preparation, ^{1}H NMR spectra were recorded on a Bruker Avance 600 spectrometer equipped with a 14 T superconducting magnet and two 5 mm probes. Analyzed samples were dissolved in deuterated chloroform (CDCl3) using tetramethylsilane as reference. Measurements were performed at 300 K using a simple pulse-acquire sequence.

2.2.12. Cocrystal physical stability under several conditions

The solid-state stability of the cocrystal solvate was analyzed at room temperature (20 °C) by storing the sample for 24 months in a desiccator containing calcium chloride. Periodically (every 3 months) and at the end of this period, the stored sample was analyzed by means of PXRD, applying the operating conditions reported in section 2.2.2.

Solid-state changes possibly caused by mechanical stresses were tested by compressing PZQ-NCM-AA at 10 Ton for 3 min, and by grinding the sample for 200 min at 25 Hz.

Further, the stability of the new system was also evaluated by storing for 6 months at 75 % RH at room temperature, in a sealed enclosure containing a saturated aqueous NaCl solution [45].

2.2.13. *In vitro and in Vivo activity*

In vitro experiments were conducted in accordance with the local cantonal veterinary guidelines, license number 520. The *in vitro* anthelmintic activity of the cocrystal solvate was tested using Newly Transformed Schistosomula (NTS), which are immature Schistosoma, and adult Schistosoma *mansoni* (S. *mansoni*).

NTS and adult *S. mansoni* were obtained by transforming cercariae from infected *B. glabrata* snails. Adult S. *mansoni* of both sexes were collected from the hepatic portal system and mesenteric veins of infected mice.

Around 50 NTS were placed in each well of a 96-well plate with culture medium and the test compound for a final well volume of 200–250 μL. Culture medium was composed of M199 medium (Gibco, Waltham MA, USA) supplemented with 5 % fetal calf serum (iFCS, 100 U/mL), 1 % penicillin/streptomycin mixture (Invitrogen, 100 U/mL) and 1 % Mäser Mix. Each compound was tested in triplicate and repeated. NTS incubated with no more than 1 % DMSO served as control. NTS were kept in the incubator at 37 °C and 5 % CO_2 for up to 72 h.

3 pairs of adult worms were placed in each well of a 24-well plate with 2–2.5 mL culture medium and the test compound. Culture medium was composed of RPMI 1640 (Invitrogen, Carlsbad, CA) supplemented with 5 % horse serum (Gibco, Waltham MA, USA) and 1 % penicillin/streptomycin mixture (Invitrogen, 100 U/mL). Each compound was initially tested in duplicate and repeated. Schistosomes incubation with no more than 1 % DMSO served as control. Worms were kept in an incubator at 37 °C and 5 % CO_2 for up to 72 h.

Worms and NTS are scored as 0 = dead; 0.25–1 = reduced motility and significant tegument damage; 1.25–2 = reduced motility or marked tegument damages 2.25–3 = viable, nice tegument, good motility.

IC_{50} values were calculated using the CalcuSyn software (ComboSyn Inc., Paramus, NJ., USA).

For the *in vivo* studies groups of 4 infected NMRI mice characterized by a patent S. *mansoni* infection (23 days postinfection) were treated orally with the test drugs via single oral doses (400 mg/kg) as oily suspensions. Untreated mice (n = 4) served as controls.

Three weeks post-treatment, animals were sacrificed by the CO_2 method and dissected. Worms were sexed and counted [46].

Worm burdens of treated mice were compared to those of control animals, and reductions of worm burden (WBR %) were calculated. A Kruskal Wallis Test was used to compare the statistical significance between the treatment and control groups.

3. Results and discussion

In our previous study [25], which resulted in a binary antiparasitic cocrystal of PZQ and NCM (CSD refcode RIPFOP01), we observed the formation of a drug-drug binary cocrystal, which we are aiming to transform into a ternary cocrystal solvate with AA, due to the inherent interest of AA as anthelmintic molecule recently recognized [20]. During exploratory studies, we noticed traces of a new solid phase when combining PZQ and NCM by liquid-assisted grinding (LAG) with AA (as visible in Fig. S1 in the Supporting Information file (SI). Via preliminary mechanochemical trials and characterization analyses (which will be detailed in this work), we determined that the correct molar ratio for the new system was PZQ-NCM-AA 1:1:1 (see Fig. S2 in the SI file as example of characterization analyses performed).

According to the ICH Q3C guidelines, which establish limits on residual solvents in pharmaceutical products, AA is classified as a Class 3 solvent, indicating a low toxicological risk. It can be used at levels up to 50 mg/day without requiring justification [3]. Considering the stoichiometric content of AA in the cocrystal solvate and the high therapeutic dose of praziquantel (PZQ) for Schistosoma infection (600 mg) [47,48], the investigated solvate would contain approximately 100 mg of AA. However, since it is reasonable to assume that the therapeutic dose of PZQ may be reduced due to the concomitant presence of NCM and AA itself, it is likely that the AA content will fall within the limits established by the aforementioned ICH guidelines. This will be confirmed following efficacy studies.

Interestingly, during the mechanochemical screening, we observed that milling for 120 min in equimolar ratio the three coformers (i.e, 195.4 mg of PZQ, 204.6 mg of NCM and 38 μL AA) led to the formation of a PZQ-NCM-AA 1:1:1 solid phase plus visible residues of the previously reported binary solid phase PZQ-NCM 1:3 anhydrous cocrystal (hereinafter referred to as its CCDC refcode RIPFOP01 [25]) (see Fig. S3 in the SI file). Through a series of additional screening experiments, we observed that the appropriate volume of AA for obtaining the cocrystal solvate was 160 μL, which largely exceeds the equimolar ratio among the components (approximately to 4.5 mmol of AA for 1 mol of PZQ and NCM). The need of such a large amount of AA cannot be explained only to the evaporation of the volatile solvent. A more plausible explanation would be that AA acts both as a reactant for the inclusion into the multicomponent solid and as a liquid that facilitates the mechanochemical reaction. While the importance of the volume of the liquid additive during mechanochemical synthesis of anhydrous multicomponent solids has been already reported [49–51], in the present study we extend such observation also for the crystallization of solvate phases.

3.1. *Synthetic routes for preparing PZQ-NCM-AA cocrystal solvate*

Given our previous knowledge of the solid-state landscape of PZQ, NCM and AA, having already synthetized some binary combinations of these coformers [15,25], and considering the high versatility of mechanochemistry [52–54], which allows the combination of multiple techniques within the same process, we decided to explore five mechanochemical synthetic routes to obtain the cocrystal solvate as pure as possible. The results are summarized in Fig. 2. Interestingly, all five explored strategies successfully resulted in the formation of the cocrystal solvate with very high yield, except for minor traces of RIPFOP01, in some synthetic routes.

Indeed, we started assembling the 3 individual coformers using the classic LAG method for 120 min (with the previously mentioned excess volume of 160 μL of AA). Through this strategy, we still noticed consistent traces of RIPFOP01 (red strategy in Fig. 2).

The second synthetic route (pink strategy in Fig. 2) encompassed the use of preformed PZQ-NCM 1:3 anhydrous cocrystal, pure PZQ Form A (to reach the PZQ-NCM equimolar ratio) and 160 μL of AA. In such conditions, the best results were obtained with 120 min of milling.

A third approach consisted of the use of preformed PZQ-AA monosolvate [15] plus an equimolar ratio of solid NCM and 160 μL of AA. In such conditions, the best result was achieved within only 60 min of milling (black strategy in Fig. 2).

In the fourth (violet) strategy, a PZQ-NCM 1:1 coamorphous was used as starting material for the synthesis of the cocrystal solvate. This intrinsically reactive solid system [55] was chosen as starting point of the solvation reaction, adopting the same rationale as in Zanolla's work [56], where, to hydrate PZQ Form A, a two-step grinding mixed process has been carried out, under neat conditions, followed by LAG conditions. A homogenous amorphous PZQ-NCM 1:1 binary system was obtained by NG for 4h. The typical halo diffusion characteristic of amorphous materials was documented using laboratory PXRD and confirmed with Synchrotron PXRD. SSNMR confirmed the formation of a new solid, as it showed no signals attributable to the starting materials and exhibited the typical broadening of signals seen in amorphous solids (LWHM ~280 Hz). SEM image showed the absence of a crystalline habitus. Most importantly, the DSC curve exhibited a unique Tg (59.09 °C), confirming the formation of a homogeneous binary system (see Fig. S4 in the SI file for the results of these analyses). This new solid was then added of 160 μL of AA to perform the cocrystal synthesis. The cocrystal solvate was

obtained after just 30 min of grinding.

A fifth synthetic route (blue strategy) involved PZQ and NCM individual coformers in equimolar ratio (with the previously mentioned excess volume of AA of 160 μL) in the presence of seeds of preformed cocrystal solvate (10 % wt). In this pathway, the most crystalline cocrystal solvate with minor traces of RIPFOP01was obtained with 120 min of milling.

Thus, we demonstrated a strategy for synthesizing ternary cocrystals by using not only individual coformers but also starting from preformed building blocks. This approach allows for a more versatile and efficient pathway to achieve the desired cocrystal solvate. Specifically, we assembled different building blocks, including the three pure coformers as well as various preformed combinations. Through these five different combinations, we were able to consistently obtain the same cocrystal solvate with very high yield and to identify the best synthetic strategy to achieve the desired cocrystal solvates as a pure phase (as attested from Synchrotron X-ray powder diffraction, in section 3.3).

The cocrystal solvate was obtained in a 100 % pure phase by adding to the preformed PZQ-AA monosolvate an equimolar ratio of solid NCM and 160 μL of AA (black strategy).

These results highlight the flexibility and robustness of our puzzle-approach, enabling the optimization of the synthesis process and the selection of the most efficient combination of starting materials.

For comparative purposes, slurry experiments were also performed (grey strategies). However, the suspension-phase synthetic routes, which were fewer in number and involved significantly longer times (7 days), were unsuccessful as they consistently produced only the binary system (RIPFOP01).

Fig. 2 shows a cartoon which reports all the synthetic pathways explored through mechanochemistry and slurry to get the new cocrystal solvate.

Even though the ternary solid was crystallized through all five investigated routes, a pure phase was obtained by milling the preformed PZQ-AA monosolvate and raw NCM in an equimolar ratio with the addition of 160 μL of AA. The time needed for completing the solid-state reaction was only 60 min.

The comprehensive characterization, presented below, was exclusively performed on the pure cocrystal solvate obtained from the best synthetic route. The new crystalline phase at the end of the mechanochemical process appeared as a white powder.

3.2. Cocrystal solvate characterizations

3.2.1. Laboratory PXRD analysis

The laboratory diffraction patterns of PZQ, NCM, PZQ-NCM-AA cocrystal solvate are shown in Fig. 3. The diffraction pattern of pure PZQ-NCM-AA shows reflections at 3.68, 4.33, 5.92, 7.10, 7.40, 14.20, 15.60, 17.70° 2θ, which are distinctly different from those of the starting materials. The absence of signals corresponding to PZQ-NCM 1:3 anhydrous cocrystal further confirms the purity of the new solid phase.

3.2.2. Synchrotron X-ray diffraction and solution of the crystal structure

The crystal structure of the cocrystal was solved from the synchrotron X-ray powder diffraction data, presented in Fig. 4. The sample showed high crystallinity, and the indexing has been performed using the program EXPO2014 [31]. The samples resulted in a *P*-1 triclinic unit cell (Fig. 5) with the following parameters: a = 6.780(1) Å, b = 16.308 (5) Å, c = 16.508(5) Å, α = 107.3089(8) °, β = 92.409(1)°, γ = 91.873(1) density = 1.339 g/cm^3 and volume 1739.37(3) Å^3, The number of formula units (1PZQ:1NCM:1AA) per unit cell is Z = 2, containing one independent molecule of PZQ, one independent molecule of NCM and one independent molecule of solvent AA in agreement with SSNMR results (see below). A first whole powder pattern fitting (Pawley method) on the experimental powder pattern resulted in a good Rwp of

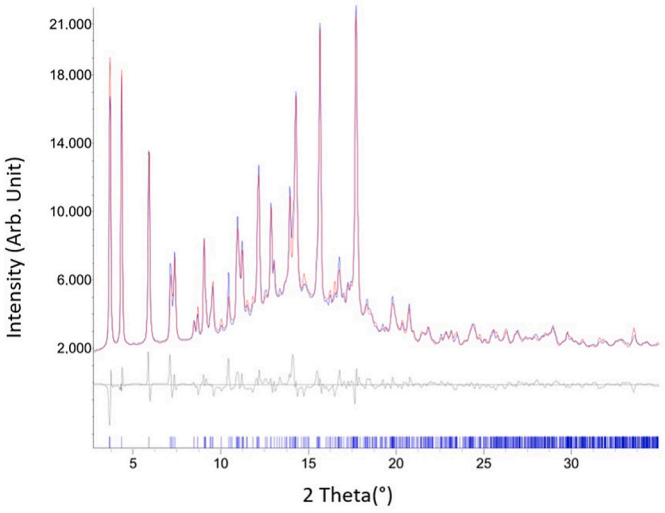

Fig. 4. Rietveld refinement profile fit (obtained after the simulated annealing with EXPO14) of the cocrystal: in blue the experimental pattern (recorded using Synchrotron radiation, wavelength: 1.00 Å), in red the calculated one. The residuals are displayed on the bottom in grey and the reflection ticks in blue. The hump centered at 15° of 2θ is due to the capillary sample holder used to perform the measurement. (For interpretation of the references to color in this figure legend, the reader is referred to the Web version of this article.)

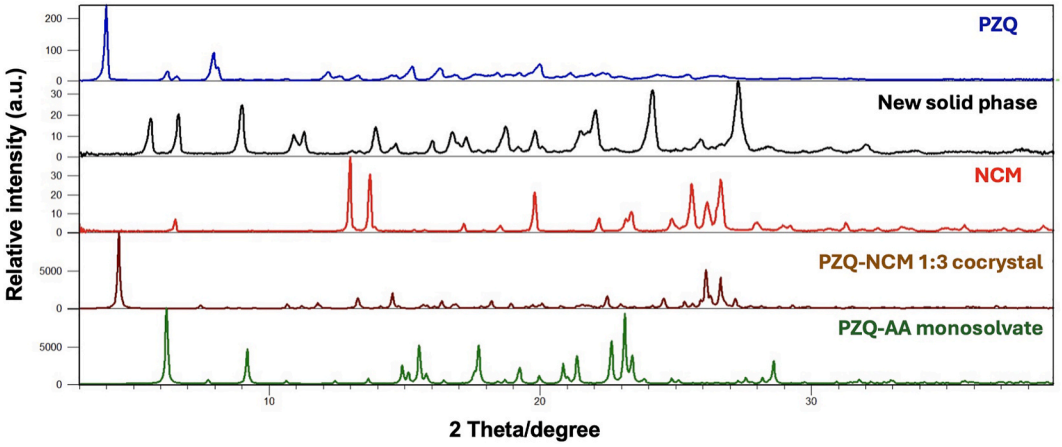

Fig. 3. PXRD of PZQ (blue), NCM (red), PZQ-NCM 1:3 anhydrous cocrystal (brown), PZQ-AA monosolvate (green) and the new phase obtained mechanochemically (black). (For interpretation of the references to color in this figure legend, the reader is referred to the Web version of this article.)

1.36 %. The final Rietveld refinement, where soft restrains on the atom distances (±0.03 Å) and angles (±0.1°) were applied, was performed in TOPAS V5 resulted in an R-Bragg factor of 3.32 %.

The cocrystal packing is showed in Fig. 5, while Table 1 reports geometrical parameters of hydrogen bonds. In this structure the cocrystal partners are tightly bounded through H-bond and molecules are coplanar. Particularly, PZQ carbonyl groups adopt the less preferred *syn* conformation in the cocrystal solvate. Similar H-bond take place between PZQ and NCM as has been founded in the anhydrous 1:3 PZQ-NCM cocrystal [25].

The powder structure resolved by the Synchrotron data has been confirmed by the DFT simulation (see section 3.8).

3.2.3. Thermal analyses

Fig. 6 shows the DSC curve of the new system, compared to pure PZQ and NCM. Specifically, the cocrystal solvate is characterized by an endothermic event at 111.11 ± 0.25 °C (enthalpy of 88.98 ± 15.56 J/g), expressed as peak temperature, which was attributed to the desolvation process. Subsequently, the solid collapses, showing no melting events for either PZQ or NCM, whose melting points are usually detected at 141 °C and 230 °C, respectively [57,58].

The TGA analysis revealed one distinct event corresponding to a weight loss of 9.77 ± 0.18 % (Fig. S5 in the SI file) (theoretical value calculated from the molecular weights: 8.56 %). The first derivative of the TGA curve showed a sharp peak at 107.23 ± 2.00 °C, confirming that the weight loss corresponded to the desolvation event already observed as an endothermic peak in the DSC curve.

3.2.4. FT-IR analysis

A detailed comparison between the spectrum of the PZQ-NCM-AA 1:1:1 cocrystal solvate shown in Fig. 7 compared to the spectra of the starting materials brings to the following observations:

- In the region from 3300 to 3000 cm^{-1}, the two bands at 3242.7 cm^{-1} and 3199.5 cm^{-1}, corresponding to the -NH stretching of NCM [59], are absent in the cocrystal solvate spectrum, testifying the involvement of the -NH amine group of NCM in hydrogen bonding.
- The band at 897 cm^{-1}, corresponding to the -NH bending of NCM [59], converts into a doublet at 893 and 886 cm^{-1} in the cocrystal solvate spectrum, further supporting the observed changes in -NH stretching.
- The complex bands at 2800-2400 cm^{-1} range, typically related to the O-H stretching vibrations in AA [60], are absent in the cocrystal solvate spectrum, indicating the involvement of hydroxyl groups in interactions.
- In the cocrystal solvate, two bands are observed at 1681 cm^{-1} and 1618 cm^{-1}, which are attributed to the two C=O stretching of PZQ initially at 1647 and 1624 cm^{-1} [61]. This can be explained by the involvement of both C=O groups in hydrogen bonding, as observed in the crystal lattice.
- The C-OH stretching of NCM, initially at 1192 cm^{-1} [62], shows a small shift.

Table 1
Geometrical parameters of hydrogen bonds found in cocrystal solvate at 298K. Atom naming in use is shown.

D-H···A	d(D-H) (Å)	d(H···A) (Å)	d(D···A) (Å)	<(DHA) (°)
O7-H33···O2	0.99(1)	1.90(9)	2.89(5)	170.1(13)
O5-H25···O1	0.97(2)	2.00(9)	2.95(10)	166(4)
N3-H26···O5	1.02(2)	1.55(3)	2.40(3)	135(16)

The FT-IR spectrum of the cocrystal solvate aligns perfectly with the interactions observed in the crystal lattice: one of the C=O groups of PZQ interacts with the -OH of AA, while the other with the -OH of NCM. Additionally, the shift observed for the N-H signal of NCM corresponds to the intramolecular interaction with the -OH group of the same NCM molecule, as seen in the crystal structure.

3.2.5. SSNMR analysis

The ^{13}C CPMAS spectra of PZQ, NCM, PZQ-NCM-AA cocrystal solvate, PZQ-NCM 1:3 anhydrous cocrystal and PZQ-AA monosolvate are shown in Fig. 8. Details about ^{13}C chemical shifts (ppm) for PZQ, NCM and PZQ-NCM-AA are reported in Table 2.

PZQ-NCM-AA cocrystal solvate spectrum appears different from the spectra of the pure PZQ and NCM (see also Fig. S7 in the SI file), confirming the formation of a new system; the absence of residual signals of PZQ – in particular those at 165.8, 55.5, 47.9 and 38.1 ppm – and of

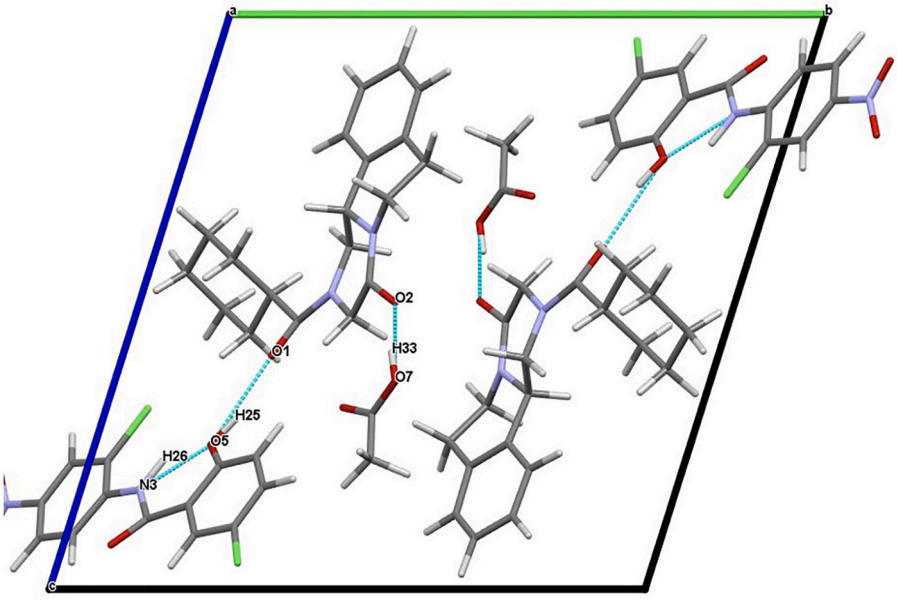

Fig. 5. Capped-stick representation of the proposed structure of PZQ-NCM-AA viewed along *a* axis. H-bonds showed with dashed blue lines. Atom color scheme: chlorine (green), nitrogen (purple), oxygen (red), carbon (grey), and hydrogen (white). (For interpretation of the references to color in this figure legend, the reader is referred to the Web version of this article.)

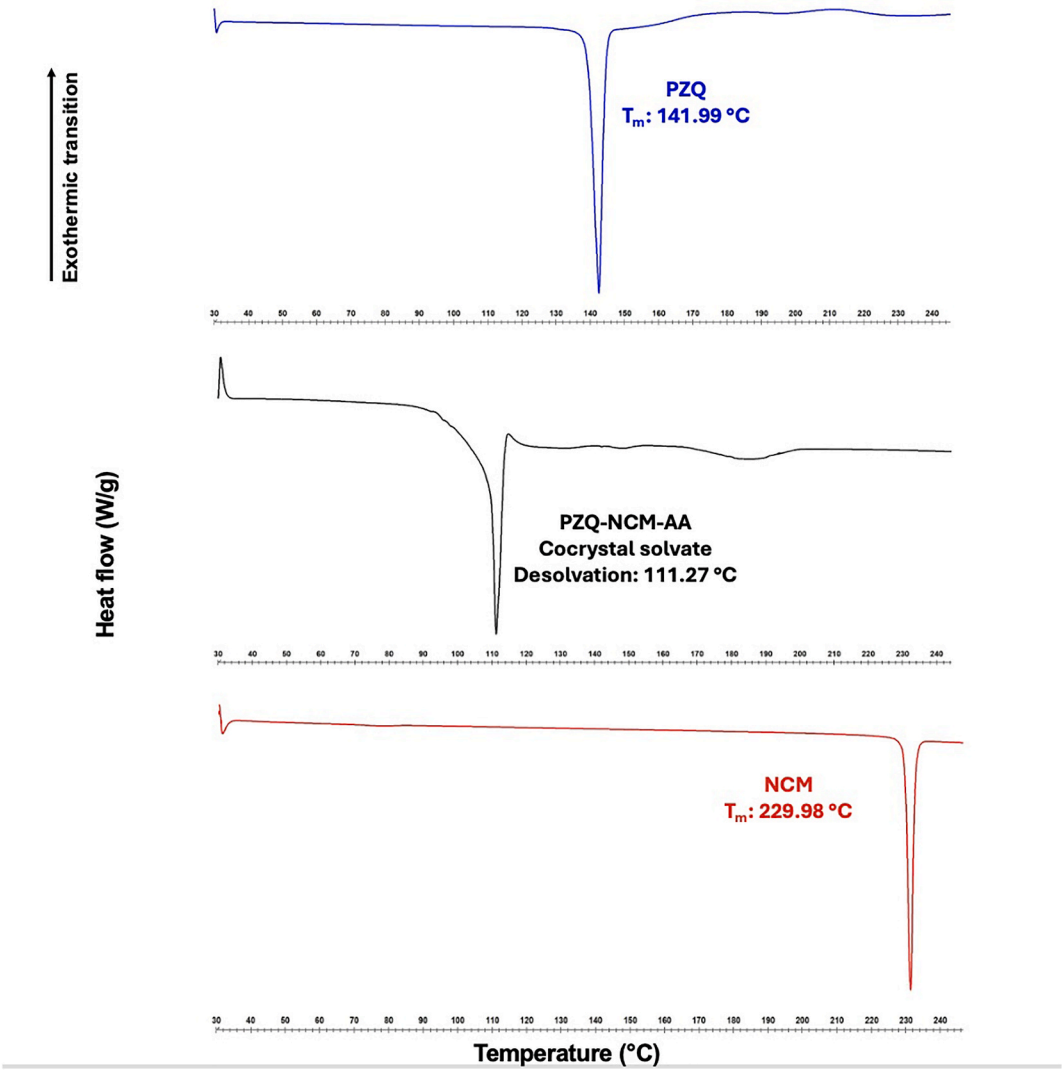

Fig. 6. DSC curves of mechanochemically prepared PZQ-NCM-AA cocrystal solvate (black), raw PZQ (blue) and raw NCM (red). (For interpretation of the references to color in this figure legend, the reader is referred to the Web version of this article.)

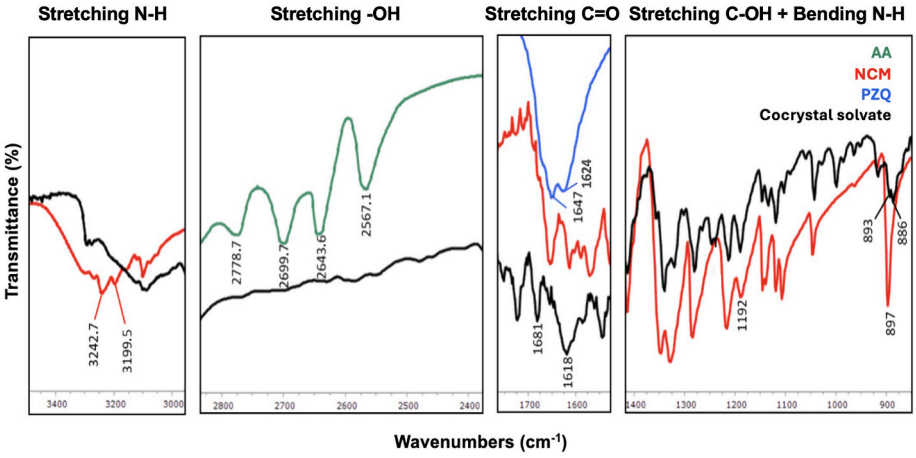

Fig. 7. FT-IR spectra of PZQ (blue), NCM (red), AA (green) and PZQ-NCM-AA cocrystal solvate (black).
(the complete spectra are reported in Figure S6). (For interpretation of the references to color in this figure legend, the reader is referred to the Web version of this article.)

NCM – in particular those at 153.9, 139.9 and 117.4 ppm – highlight that there is no presence of pristine PZQ and NCM. The purity of this new solid phase is further confirmed by the absence of signals corresponding to PZQ-NCM 1:3 anhydrous cocrystal – especially that at 161.5, 154.1, 151.8, 138.2, 115.0 ppm – and to PZQ-AA solvate – particularly that at 172.2, 134.8, 53.7 and 37.2 ppm (see also Fig. S8 in SI).

The presence of AA can be observed from the peak at 20.2 ppm corresponding to the CH_3 group, highlighted in Fig. 8 with a green arrow. The AA carbonyl group is visible as shoulder around 173.7 ppm, see green arrow in Fig. 8.

The number of signals in the PZQ-NCM-AA cocrystal solvate spectrum suggests the presence of one independent molecule of PZQ, one of NCM and one of AA, confirmed also from ^{1}H NMR analysis (see below).

3.2.6. ^{1}H NMR analysis

The ^{1}H NMR spectrum of PZQ-NCM-AA cocrystal solvate is reported in Fig. S9 in SI. The integrations of the signals at 2.6 and 2.5 ppm, corresponding to PZQ H4 (it is split due to the presence of two coformers of PZQ [64]), at 8.7 ppm, related to an aromatic CH of NCM, and at 2.1 ppm, corresponding to the three protons of the CH_3 of AA, confirm the stoichiometric ratio of 1PZQ:1NCM:1AA, in agreement with Synchrotron X-ray powder diffraction results.

3.2.7. DFT calculations

The initially Rietveld refined structure was re-optimized at DFT level with Quantum Espresso and submitted for a second refining. This "quasi self-consistent" process, which combines experimental and theoretical data, has proven to be very useful in helping to refine the resolution of particularly difficult structures [65,66]. The final structure has been optimized with a fixed cell scheme, in which only atoms were allowed to move, while the cell shape and volume were kept constant. The comparison between the experimental data and the simulated one (fixed cell) is shown in Fig. 9. The root-mean-square error (RMSE) relative to the overlap between the two structures was calculated by the crystal packing similarity tool implemented in Mercury and it is 0.245, typical of reliable structures [67]. It should be mentioned, however, that full free cell optimization resulted in a structure very similar to the experimental one (RMSE = 0.245), which indicates a very good agreement with the theoretical structure computed at 0 K. To further validate the structure from powder data the experimental and computed chemical shifts (see Table 2) were compared and a low ^{13}C RMSE (2.13) was obtained. Fig. S10 in the SI file displays the good correlation between the experimental and computed chemical shifts.

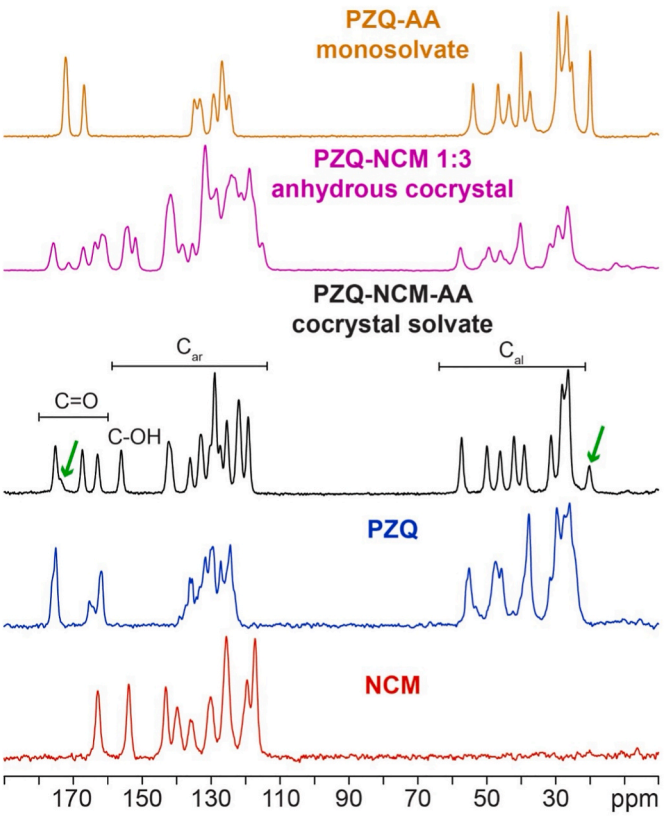

Fig. 8. ^{13}C (150.91 MHz) CPMAS spectrum of PZQ-NCM-AA cocrystal solvate (black), acquired at a spinning speed of 20 kHz at room temperature, compared to ^{13}C (100.63 MHz) CPMAS spectra of pure NCM (red), pure PZQ (blue), PZQ-NCM 1:3 anhydrous cocrystal (pink), acquired at a spinning speed of 12 kHz at room temperature, and ^{13}C (150.91 MHz) CPMAS spectrum of PZQ-AA monosolvate (orange), acquired at a spinning speed of 20 kHz at room temperature. The two green arrows highlight the signals attributed to AA. (For interpretation of the references to color in this figure legend, the reader is referred to the Web version of this article.)

Table 2
Experimental (exp)^{13}C chemical shifts (ppm) for PZQ [57], NCM [63] and PZQ-NCM-AA and computed (calc)^{13}C chemical shifts (ppm) for PZQ-NCM-AA, with assignments.

Group	Atom	PZQ exp	NCM exp	PZQ-NCM-AA exp	PZQ-NCM-AA calc
C = O	1	175.4, 176.2 sh		175.2	176.02
C = O	14	165.8, 164.6, 162.1		167.4	166.56
C_q	12	137.7, 136.5		133.1	134.52
C_q	11	135.8, 134.6		129.0	129.27
CH	8	129.7, 127.5, 124.8		130.1	131.02
CH	18	133.7		122.0	126.72
CH	19	132.0		129.0	129.23
CH	7	130.5		127.4	129.2
CH	17	56.3, 55.5		57.3	56.92
CH_2	15	46.1		46.2	43.34
CH_2	16	47.9		50.0	48.03
CH	4	39.7		42.1	40.57
CH_2	10	38.1		39.1	36.34
CH_2	3	32, 30.1, 27.9,		31.3	29.51
CH_2	5	26.3, 25.3		28.1	26.94
CH_2	9			28.1	25.15
CH_2	13			26.4	23.68
CH_2	6			26.4	24.36
CH_2	2			26.4	24.29
C = O	7′		162.9	163.0	163.24
C - OH	13′		153.9	156.1	159.04
C - NO_2	4′		143.3	142.3	143.44
C - NH	1′		139.9	142.3	142.49
CH_{Ar}	12′		136.1, 130.3,	119.2	119
	11′		125.7, 119.7	136.1	137.63
	9′			133.1	133.18
	3′			122.0	123
	5′			125.5	128.68
	6′			122.0	121.63
C - Cl	10′		129.8 sh	129.0	131.33
	2′			125.5	127.68
C - CO	8′		117.4	119.2	118.31
COOH	1″			173.7	177.8
CH_3	2″			20.2	15.66

3.2.8. SEM analysis

SEM images of powders of PZQ, NCM and PZQ-NCM-AA cocrystal solvate are reported in Fig. 10. The new system is composed of agglomerates of small thin plates (with an approximate diameter less than 1 μm), exhibiting a habitus distinctly different from the needle-shaped particles typically observed in PZQ [68] and the rectangles with protrusions characteristic of NCM [69].

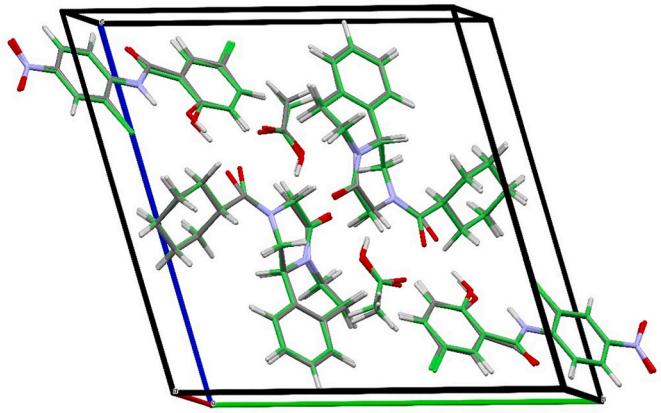

Fig. 9. Overlap conformations between the experimental refined crystal structures (red) and the computed one (fixed cell) by DFT (cyano). (For interpretation of the references to color in this figure legend, the reader is referred to the Web version of this article.)

3.2.9. Drug recovery

^{1}H NMR spectroscopy was also used to determine whether component degradation occurs after different synthetic procedures. The spectra of pure PZQ, NCM, with two samples of PZQ-NCM-AA cocrystal solvates, which only differ from the process used for obtaining the solid product, were compared (Fig. S11). One sample was obtained through the synthesis reported in section 2.1.1.1and the other one following the procedure of section 2.1.1.4. Spectroscopic evaluations have shown no evidence of PZQ degradation upon grinding in the presence of NCM and AA, even though is well-known from literature the PZQ propensity to degradation when ground in the presence of other substances, with the insurgence of peculiar degradation products as a function of the excipient used [68,70,71].

3.2.10. Physical stability under several conditions

The stability of solvates is a critical aspect of pharmaceutical science, since these materials are inherently prone to desolvation, a process where the solvent molecules are expelled from the crystal lattice, often leading to significant structural and thermodynamic changes which result in potential loss of desired properties [72,73].

In the present case, the physical stability of the cocrystal solvate was assessed under various conditions. The main objectives were to determine if there were signs of (spontaneous or induced) desolvation leading to cocrystal dissociation or conversion into the corresponding PZQ-NCM anhydrous cocrystal, and to evaluate if the new system could prevent the formation of the insoluble NCM monohydrate, which typically occurs within a month of exposure to ambient humidity [58].

Under static conditions (i.e., 20 °C, 0 % RH), the new multicomponent crystal remained stable for 24 months with no signs of cocrystal dissociation or conversion into the anhydrous cocrystal (see Fig. S12 in the SI file). During this period, the sample retained its white crystalline powder appearance, unlike the samples containing trace amounts of RIPFOP01 (obtained by the other synthetic routes), which exhibited a pinkish hue during storage under similar conditions (Fig. S13 in the SI file). Interestingly, this pink coloration could not be attributed to RIPFOP01 itself (reported to be a white powder [25]), nor to impurity B of PZQ (as demonstrated by ^{1}H NMR analysis), which is indeed reported to be a pink solid [74]. A plausible explanation of the appearance of such coloration, therefore, is still missing.

Additionally, the physical stability of PZQ-NCM-AA upon mechanical stress was also evaluated since it is well known that solvates tend to desolvate and undergo structural relaxation when subjected to compression, which can significantly impact their physical stability and performance [75–77]. We therefore evaluated the physical stability of the cocrystal solvate under compression to better understand its behavior under potential practical pharmaceutical manufacturing conditions.

Specifically, the solid was subjected to compression under the same operating conditions used for creating KBr discs for FT-IR analysis (see section 2.2.6). In this case, mechanical compression did not cause any dissociation or the formation of other phases, as evidenced by PXRD, however, DSC analysis indicated a reduction in the overall crystallinity of the sample (see Fig. S14 in the SI file).

The mechanical resistance was also tested through milling the cocrystal solvate for 200 min at 25 Hz, following the procedure adopted by Zanolla and coauthors [15]. The PXRD and DSC results demonstrated that, despite the cocrystal solvate being subjected to intense and impactful mechanical stress, the new phase remained almost intact. Only partial desolvation with conversion into the corresponding PZQ-NCM 1:3 anhydrous cocrystal was observed, as could be expected (Fig. S15 in the SI file).

PZQ-NCM-AA cocrystal solvate was also placed for 6 months in a sealed enclosure with a saturated aqueous NaCl solution (75 % RH) and periodically analyzed by means of PXRD. These analyses were carried out as the phenomenon of cocrystal dissociation at high humidity is well known [78]. Further, the possibility of the formation of NCM monohydrate is a constant risk when handling this drug [58,69]. The new ternary cocrystal remained stable throughout the entire six-month period under such conditions (Fig. S16 in the SI file). Importantly, the conservation of the powdered material at high humidity conditions did not bring in the typical greenish color of NCM monohydrate. This is, therefore, one of those cases where cocrystallization enhances the physical stability of moisture-sensitive drugs [79].

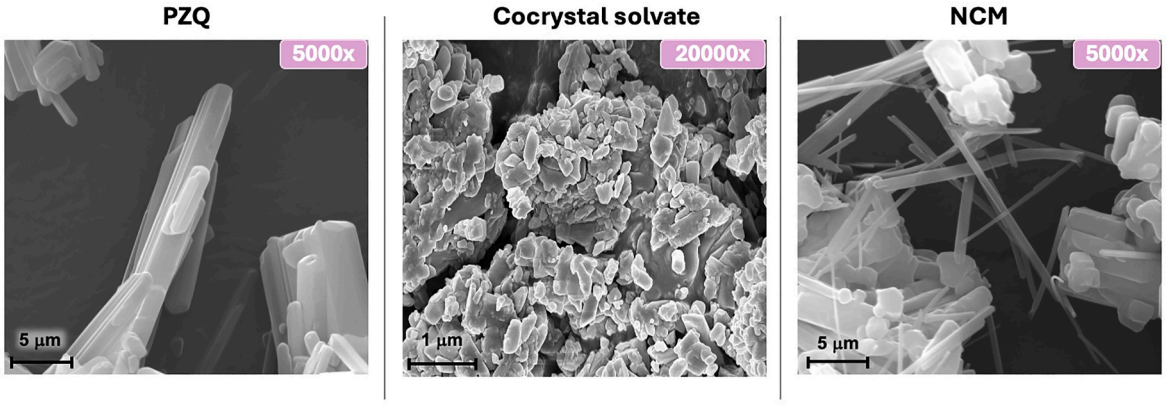

Fig. 10. SEM images of (a) PZQ (5000x), (b) PZQ-NCM-AA cocrystal solvate (20000x) and (c) NCM (5000x).

3.2.11. In Vitro activity

The new cocrystal solvate revealed the highest activity against both NTS and adult *S. mansoni* (Table 3). Concentrations of 0.1–10 μM resulted in death of all worms. A concentration of 0.01 μM revealed an activity of 41.7 % (NTS) and 53.7 % (adult worms). This translates to IC50 values of 0.01 μM against adult worms and NTS, respectively. For comparison, against NTS, pure PZQ and NCM, binary PZQ-NCM cocrystal and PZQ-AA monosolvate showed a 10-fold lower activity, i.e., were only active at 1 and 10 μM – Against adult worms only NCM and the PZQ-NCM cocrystal showed a similar good performance as the new cocrystal solvate with moderate activity still observed at 0.01 μM.

3.2.12. In Vivo preliminary studies

In a pilot study, the cocrystal solvate was orally administered as an oily suspension to a group of four mice infected with a patented S. *mansoni* infection, at a single dose of 400 mg/kg. Twenty-three days post-infection, the mice treated with the cocrystal solvate showed a statistically significant ($p < 0.05$) 74.3 % reduction in worm burden, compared to approximately 87 % in mice treated with the original PZQ in a previous study [80] (Table 4). These results suggest that the cocrystal solvate retains its antischistosomal activity relative to the raw PZQ.

The *in vitro* activity tests were promising, as the three active pharmaceutical ingredients (APIs) in the new multicomponent system appeared to exert a synergistic effect. The hypothesis proposed in the introductory section of the results has been confirmed by efficacy studies, demonstrating that the therapeutic dose of PZQ may be reduced due to the synergistic effect of NCM and AA.

The discrepancy between the *in vitro* and *in vivo* results could potentially be attributed to the vehicle used for administration; the cocrystal solvate was difficult to disperse in corn oil, resulting in a cloudy suspension with sediment rather than a clear homogeneous suspension, which would have guaranteed an accurate dosage.

Moreover, the use of an oil-based vehicle suspension, although better than the aqueous-based one, may not be ideal for showcasing the full potential of the cocrystal, which would likely benefit from being administered in a solid form, such as in minicapsules of size M. However, the minicapules are very difficult to administer to mice, as observed in the previous study, where many animals died during administration [25]. Future *in vivo* studies should be conducted using minicapsules size M, following thorough training and refinement of the administration technique for these pharmaceutical forms.

4. Conclusions

In this paper, we reported a cocrystal solvate composed of praziquantel, niclosamide and acetic acid, all having documented anthelmintic properties. The ternary cocrystal exhibited largely superior anthelmintic activity against *in vitro* Schistosoma *mansoni* adults and, notably, against Newly Transformed Schistosomula compared to pure individual drugs (i.e., PZQ and NCM) and to its binary counterparts (i.e., PZQ-NCM cocrystal and PZQ-AA monosolvate).

Mechanochemical methods demonstrated a great potential by successfully producing the new system across five different routes. A pure phase was achieved by milling for 60 min preformed praziquantel-acetic acid monosolvate and raw niclosamide in an equimolar ratio. For completing the mechanochemical reaction, 160 μL of acetic acid were needed, since the solvent acted both as a solvate-forming molecule and as a liquid additive.

On the contrary, slurry experiments, performed for comparative purposes, were unsuccessful.

The structure of the cocrystal solvate was successfully solved and refined from the Synchrotron PXRD data, with the support of theoretical periodic calculations and an integrated SSNMR approach. The new system crystallizes in the triclinic space group of *P*-1, showing one praziquantel, one niclosamide and one acetic acid molecules linked through homo- and heteromolecular hydrogen bonds in the asymmetric unit. Spectrometric evaluations have shown no evidence of degradation of praziquantel upon grinding. Such observation is important considering the well-known tendency of this molecule to degrade under mechanochemical processing in the presence of excipients.

The new multicomponent crystal remained stable for 24 months at ambient temperature and demonstrates physical stability under high relative humidity conditions (75 % RH), effectively preventing the formation of the well-known niclosamide monohydrate, which typically forms within just one month of air exposure at room temperature. Analysis of solid-state transformations after mechanical treatments revealed that extended grinding (200 min) just led to a decrease of crystallinity degree, whereas compression (10 Ton for 3 min) just promotes a partial conversion in the praziquantel-niclosamide 1:3 anhydrous cocrystal.

However, the most important aspect of this higher-order crystal remains— as mentioned above— the anthelmintic activity enhancement compared to the individual active ingredients and their binary counterparts (PZQ-NCM cocrystal and the PZQ-AA monosolvate).

The drastic reduction in IC50 (0.01 μM against Newly Transformed Schistosomula and S. *mansoni* adult) of the new solid fully justifies the ambitious challenge of incorporating more than two components into a single crystalline phase, underscoring the pivotal role of the ternary system in enhancing bioactivity. This finding highlights the need to tackle the next challenge: identifying the most suitable oral dosage form for a cocrystal, a requirement that remains unmet in the pilot studies conducted in this work.

Table 4
Effect of the cocrystal solvate (administered as oily suspension at a single cocrystal dose of 400 mg/kg) on the worm burden reduction (WBR) in mice harboring a chronic S. *mansoni* infection.

Sample	Average of WBR %	Number of mice
Control	–	4
PZQ-NCM-AA cocrystal solvate	74.3	4

Table 3
In vitro activity of the cocrystal solvate against S. *mansoni* adult and Newly Transformed Schistosomula (NTS), compared to pure PZQ, NCM and PZQ-AA monosolvate.

S. *mansoni* adult						Newly Transformed Schistosomula				
Testconc.	Effect in % (72h) + SD				IC50 (μM) (72h) Dm	Effect in % (72h) + SD				IC50 (μM) (72h) Dm
	10 μM	1 μM	0.1 μM	0.01 μM		10 μM	1 μM	0.1 μM	0.01 μM	
New cocrystal solvate[a]	100 (0)	100 (0)	90.8 (1.9)	53.7 (5.6)	0.01	100 (0)	100 (0)	100 (0)	41.7 (1.7)	0.01
PZQ	92.1 (1.6)	92.1 (1.6)	51.1 (4.7)		0.44	82.4 (2)	70.8 (4.2)	31.3 (2.1)	82.4 (2)	
NCM	100 (0)	62.1 (1.6)	77.8 (3.2)	49.5 (0)	0.09	100 (0)	83.3 (0)	31.3 (2.1)	100 (0)	
PZQ monosolvate[b]	100 (0)	87.5 (0)	41.7 (8.3)		0.18	87.5 (0)	62.5 (0)	31.3 (2.1)	87.5 (0)	
PZQ-NCM cocrystal[c]		100 (0)	72.0 (4.0)	39.6 (6.3)	0.02			92.3 (3.8)	25.0 (1.9)	0.20

[a] The micromolar dose was calculated using cocrystal molecular weight.
[b] Obtained as previously reported [15].
[c] Taken from ref. [25].

CRediT authorship contribution statement

Ilenia D'Abbrunzo: Writing – original draft, Investigation, Conceptualization. **Lara Gigli:** Software, Investigation. **Nicola Demitri:** Software, Investigation. **Chiara Sabena:** Writing – original draft, Investigation. **Carlo Nervi:** Software, Formal analysis. **Michele R. Chierotti:** Writing – review & editing, Supervision, Resources, Funding acquisition. **Serena Bertoni:** Writing – original draft, Investigation. **Irena Škorić:** Writing – original draft, Investigation. **Cécile Häberli:** Software, Investigation. **Jennifer Keiser:** Writing – review & editing, Resources, Methodology. **Dritan Hasa:** Writing – review & editing, Supervision. **Beatrice Perissutti:** Writing – review & editing, Supervision, Resources, Project administration, Conceptualization.

Declaration of competing interest

The authors declare that they have no known competing financial interests or personal relationships that could have appeared to influence the work reported in this paper.

Acknowledgments

Authors wish to thank Paolo Pengo for kind cooperation in FT-IR analysis.

M.R.C., C.S. and C.N. acknowledge support from the project CH4.0 under the MUR program "Dipartimenti di Eccellenza 2023–2027" (CUP: D13C22003520001), the project FLIPPER (PRIN2022 n. 202224KAX8; CUP D53D23010020006) funded by European Union - Next Generation EU, Mission 4 Component 1, the project NICE (PRIN2020 n. 2020Y2CZJ2; CUP D13C22000440001).

Appendix A. Supplementary data

Supplementary data to this article can be found online at https://doi.org/10.1016/j.jddst.2025.106974.

Data availability

CCDC number 2391439 contains the crystallographic data for the cocrystal solvate, obtainable for free from The Cambridge Crystallographic Data Centre via https://www.ccdc.cam.ac.uk/structures.

References

[1] A.M. Healy, Z. Ayenew Worku, D. Kumar, A.M. Madi, Pharmaceutical solvates, hydrates and amorphous forms: a special emphasis on cocrystals, Adv. Drug Deliv. Rev. 117 (2017) 25–46, https://doi.org/10.1016/j.addr.2017.03.002.
[2] U.J. Griesser, The importance of solvates, in: Polymorphism, Wiley, 2006, pp. 211–233, https://doi.org/10.1002/3527607889.ch8.
[3] ICH Q3C (R9) residual solvents - scientific guideline | European Medicines Agency, (n.d.).https://www.ema.europa.eu/en/ich-q3c-r9-residual-solvents-scientific-guideline (accessed April 1, 2025).
[4] FDA, CDER, MEKINIST® (trametinib) tablets, for oral use, https://www.fda.gov/medwatch. (accessed June 27, 2024).
[5] FDA, CDER, FARXIGA® (dapagliflozin) tablets, for oral use, https://www.fda.gov/medwatch. (accessed June 27, 2024).
[6] FDA, CDER, JEVTANA® (cabazitaxel) injection, 60 mg/1.5 mL, for intravenous infusion only, https://www.fda.gov/medwatch. (accessed June 27, 2024).
[7] FDA, CDER, PREZISTA® (darunavir) oral suspension, for oral use PREZISTA (darunavir) tablet, film coated for oral use, https://www.fda.gov/medwatch. (accessed June 27, 2024).
[8] FDA, CDER, DOXTERICTM (doxycycline hyclate delayed-release tablets), oral use, https://www.fda.gov/drugsatfda (accessed June 27, 2024).
[9] FDA, CDER, CRIXIVAN® (INDINAVIR SULFATE) CAPSULES, https://www.fda.gov/drugsatfda (accessed June 27, 2024).
[10] FDA, CDER, COUMADIN (warfarin sodium) tablets, for oral use COUMADIN (warfarin sodium) for injection, for intravenous use, https://www.fda.gov/medwatch. (accessed June 27, 2024).
[11] C.R. Groom, I.J. Bruno, M.P. Lightfoot, S.C. Ward, The Cambridge structural database, Acta Crystallogr B Struct Sci. Cryst Eng Mater. 72 (2016) 171–179, https://doi.org/10.1107/S2052520616003954.
[12] N.J. Babu, P. Sanphui, A. Nangia, Crystal engineering of stable temozolomide cocrystals, Chem. Asian J. 7 (2012) 2274–2285, https://doi.org/10.1002/asia.201200205.
[13] A. Averdunk, E.C. Hosten, R. Betz, Crystal structure of phenarsazine chloride acetic acid solvate, C14H13AsClNO2, Z. Kristallogr. New Cryst. Struct. 236 (2021) 113–115, https://doi.org/10.1515/ncrs-2020-0434.
[14] R.M. Sweet, L.F. Dahl, Molecular architecture of the cephalosporins. Insights into biological activity based on structural investigations, J. Am. Chem. Soc. 92 (1970) 5489–5507, https://doi.org/10.1021/ja00721a032.
[15] D. Zanolla, L. Gigli, D. Hasa, M.R. Chierotti, M. Arhangelskis, N. Demitri, W. Jones, D. Voinovich, B. Perissutti, Mechanochemical synthesis and physicochemical characterization of previously unreported praziquantel solvates with 2-Pyrrolidone and acetic acid, Pharmaceutics 13 (2021) 1606, https://doi.org/10.3390/pharmaceutics13101606.
[16] Ö. Almarsson, M.B. Hickey, M.L. Peterson, S.L. Morissette, S. Soukasene, C. McNulty, M. Tawa, J.M. MacPhee, J.F. Remenar, High-throughput surveys of crystal form diversity of highly polymorphic pharmaceutical compounds, Cryst. Growth Des. 3 (2003) 927–933, https://doi.org/10.1021/cg034058b.
[17] R.M. Bhardwaj, J.A. McMahon, J. Nyman, L.S. Price, S. Konar, I.D.H. Oswald, C. R. Pulham, S.L. Price, S.M. Reutzel-Edens, A prolific solvate former, galunisertib, under the pressure of crystal structure prediction, produces ten diverse polymorphs, J. Am. Chem. Soc. 141 (2019) 13887–13897, https://doi.org/10.1021/jacs.9b06634.
[18] D. Cioli, L. Pica-Mattoccia, A. Basso, A. Guidi, Schistosomiasis control: praziquantel forever? Mol. Biochem. Parasitol. 195 (2014) 23–29, https://doi.org/10.1016/j.molbiopara.2014.06.002.
[19] D. Luedeker, R. Gossmann, K. Langer, G. Brunklaus, Crystal engineering of pharmaceutical Co-crystals: "nmr Crystallography" of niclosamide Co-crystals, Cryst. Growth Des. 16 (2016) 3087–3100, https://doi.org/10.1021/acs.cgd.5b01619.
[20] X. Tan, Y. Yan, G. Zhang, P. Li, F. Ling, T. Liu, G. Wang, Target epidermal damage of Gyrodactylus kobayashii to obtain the effective anthelmintic compound glacial acetic acid, Aquaculture 577 (2023) 739993, https://doi.org/10.1016/j.aquaculture.2023.739993.
[21] C.L. Ventola, The antibiotic resistance crisis: part 1: causes and threats, P T 40 (2015) 277–283.
[22] S.K. Ahmed, S. Hussein, K. Qurbani, R.H. Ibrahim, A. Fareeq, K.A. Mahmood, M. G. Mohamed, Antimicrobial resistance: impacts, challenges, and future prospects, J. Med. Surg Public Health 2 (2024) 100081, https://doi.org/10.1016/j.glmedi.2024.100081.
[23] SCOGS (Select Committee on GRAS substances), https://www.cfsanappsexternal.fda.gov/scripts/fdcc/?set=SCOGS&sort=Sortsubstance&order=ASC&startrow=1&type=basic&search=ACETIC%20ACID (accessed June 20, 2024).
[24] Substances Added to Food (formerly EAFUS), https://www.cfsanappsexternal.fda.gov/scripts/fdcc/?set=FoodSubstances (accessed June 20, 2024).
[25] I. D'Abbrunzo, E. Bianco, L. Gigli, N. Demitri, R. Birolo, M.R. Chierotti, I. Škoríc, J. Keiser, C. Häberli, D. Voinovich, D. Hasa, B. Perissutti, Praziquantel meets niclosamide: a dual-drug antiparasitic cocrystal, Int. J. Pharm. 644 (2023) 123315, https://doi.org/10.1016/j.ijpharm.2023.123315.
[26] T. Friščić, S.L. Childs, S.A.A. Rizvi, W. Jones, The role of solvent in mechanochemical and sonochemical cocrystal formation: a solubility-based approach for predicting cocrystallisation outcome, CrystEngComm 11 (2009) 418–426, https://doi.org/10.1039/B815174A.
[27] I. D'Abbrunzo, M. Spadaro, M. Arhangelskis, G. Zingone, D. Hasa, B. Perissutti, Competitive mechanochemical solvate formation of theophylline in the presence of miscible liquid mixtures, Cryst. Growth Des. 23 (2023) 8094–8102, https://doi.org/10.1021/acs.cgd.3c00834.
[28] A. Lausi, M. Polentarutti, S. Onesti, J.R. Plaisier, E. Busetto, G. Bais, L. Barba, A. Cassetta, G. Campi, D. Lamba, A. Pifferi, S.C. Mande, D.D. Sarma, S.M. Sharma, G. Paolucci, Status of the crystallography beamlines at elettra, Eur. Phys .J. Plus 130 (2015) 43, https://doi.org/10.1140/epjp/i2015-15043-3.
[29] A.P. Hammersley, S.O. Svensson, M. Hanfland, A.N. Fitch, D. Hausermann, Two-dimensional detector software: from real detector to idealised image or two-theta scan, High Press. Res. 14 (1996) 235–248, https://doi.org/10.1080/08957959608201408.
[30] THE FIT2D HOME PAGE, https://www.esrf.fr/computing/scientific/FIT2D/ (accessed September 10, 2024).
[31] A. Altomare, C. Cuocci, C. Giacovazzo, A. Moliterni, R. Rizzi, N. Corriero, A. Falcicchio, EXPO2013 : a kit of tools for phasing crystal structures from powder data, J. Appl. Crystallogr. 46 (2013) 1231–1235, https://doi.org/10.1107/S0021889813013113.
[32] Search results - access structures, https://www.ccdc.cam.ac.uk/structures/Search?Ccdcid=896766&DatabaseToSearch=Published (accessed September 10, 2024).
[33] BIOVIA materials studio | dassault systèmes https://www.3ds.com/products/biovia/materials-studio (accessed September 10, 2024).
[34] P. Giannozzi, S. Baroni, N. Bonini, M. Calandra, R. Car, C. Cavazzoni, D. Ceresoli, G.L. Chiarotti, M. Cococcioni, I. Dabo, A. Dal Corso, S. de Gironcoli, S. Fabris, G. Fratesi, R. Gebauer, U. Gerstmann, C. Gougoussis, A. Kokalj, M. Lazzeri, L. Martin-Samos, N. Marzari, F. Mauri, R. Mazzarello, S. Paolini, A. Pasquarello, L. Paulatto, C. Sbraccia, S. Scandolo, G. Sclauzero, A.P. Seitsonen, A. Smogunov, P. Umari, R.M. Wentzcovitch, Quantum espresso: a modular and open-source software project for quantum simulations of materials, J. Phys. Condens. Matter 21 (2009) 395502, https://doi.org/10.1088/0953-8984/21/39/395502.
[35] K. Lee, É.D. Murray, L. Kong, B.I. Lundqvist, D.C. Langreth, Higher-accuracy van der Waals density functional, Phys. Rev. B 82 (2010) 081101, https://doi.org/10.1103/PhysRevB.82.081101.

[36] I. Hamada, van der Waals density functional made accurate, Phys. Rev. B 89 (2014) 121103, https://doi.org/10.1103/PhysRevB.89.121103.
[37] G. Prandini, A. Marrazzo, I.E. Castelli, N. Mounet, N. Marzari, Precision and efficiency in solid-state pseudopotential calculations, npj Comput. Mater. 4 (2018) 72, https://doi.org/10.1038/s41524-018-0127-2.
[38] K. Lejaeghere, G. Bihlmayer, T. Björkman, P. Blaha, S. Blügel, V. Blum, D. Caliste, I. E. Castelli, S.J. Clark, A. Dal Corso, S. de Gironcoli, T. Deutsch, J.K. Dewhurst, I. Di Marco, C. Draxl, M. Dułak, O. Eriksson, J.A. Flores-Livas, K.F. Garrity, L. Genovese, P. Giannozzi, M. Giantomassi, S. Goedecker, X. Gonze, O. Grånäs, E.K.U. Gross, A. Gulans, F. Gygi, D.R. Hamann, P.J. Hasnip, N.A.W. Holzwarth, D. Iuşan, D. B. Jochym, F. Jollet, D. Jones, G. Kresse, K. Koepernik, E. Küçükbenli, Y. O. Kvashnin, I.L.M. Locht, S. Lubeck, M. Marsman, N. Marzari, U. Nitzsche, L. Nordström, T. Ozaki, L. Paulatto, C.J. Pickard, W. Poelmans, M.I.J. Probert, K. Refson, M. Richter, G.-M. Rignanese, S. Saha, M. Scheffler, M. Schlipf, K. Schwarz, S. Sharma, F. Tavazza, P. Thunström, A. Tkatchenko, M. Torrent, D. Vanderbilt, M.J. van Setten, V. Van Speybroeck, J.M. Wills, J.R. Yates, G.-X. Zhang, S. Cottenier, Reproducibility in density functional theory calculations of solids, Science 351 (2016), https://doi.org/10.1126/science.aad3000, 1979.
[39] T. Charpentier, The PAW/GIPAW approach for computing NMR parameters: a new dimension added to NMR study of solids, Solid State Nucl. Magn. Reson. 40 (2011) 1–20, https://doi.org/10.1016/j.ssnmr.2011.04.006.
[40] A. Dal Corso, Pseudopotentials periodic table: from H to Pu, Comput. Mater. Sci. 95 (2014) 337–350, https://doi.org/10.1016/j.commatsci.2014.07.043.
[41] F. Franco, M. Baricco, M.R. Chierotti, R. Gobetto, C. Nervi, Coupling solid-state NMR with GIPAW ab initio calculations in metal hydrides and borohydrides, J. Phys. Chem. C 117 (2013) 9991–9998, https://doi.org/10.1021/jp3126895.
[42] R.K. Harris, P. Hodgkinson, C.J. Pickard, J.R. Yates, V. Zorin, Chemical shift computations on a crystallographic basis: some reflections and comments, Magn. Reson. Chem. 45 (2007) S174–S186, https://doi.org/10.1002/mrc.2132.
[43] G.N.M. Reddy, A. Huqi, D. Iuga, S. Sakurai, A. Marsh, J.T. Davis, S. Masiero, S. P. Brown, Co-existence of distinct supramolecular assemblies in solution and in the solid state, Chem. Eur J. 23 (2017) 2315–2322, https://doi.org/10.1002/chem.201604832.
[44] J.K. Nimmo, B.W. Lucas, Solid-state phase transition in triethylenediamine, N (CH2CH2)3N. I. The crystal structure of phase II at 298 K, Acta Crystallogr. B 32 (1976) 348–353, https://doi.org/10.1107/S0567740876003038.
[45] L. Greenspan, Humidity fixed points of binary saturated aqueous solutions, J. Res. Natl Bur Stand [A] Phys Chem. 81 (1976) 89–96, https://doi.org/10.6028/jres.081A.011.
[46] S.-H. Xiao, J. Keiser, J. Chollet, J. Utzinger, Y. Dong, Y. Endriss, J.L. Vennerstrom, M. Tanner, In vitro and in vivo activities of synthetic trioxolanes against major human schistosome species, Antimicrob. Agents Chemother. 51 (2007) 1440–1445, https://doi.org/10.1128/AAC.01537-06.
[47] B. Gryseels, K. Polman, J. Clerinx, L. Kestens, Human schistosomiasis, Lancet 368 (2006) 1106–1118, https://doi.org/10.1016/S0140-6736(06)69440-3.
[48] J.C. Sousa-Figueiredo, M. Betson, J.R. Stothard, Treatment of schistosomiasis in African infants and preschool-aged children: downward extension and biometric optimization of the current praziquantel dose pole, Int Health 4 (2012) 95–102, https://doi.org/10.1016/j.inhe.2012.03.003.
[49] D. Hasa, E. Miniussi, W. Jones, Mechanochemical synthesis of multicomponent crystals: one liquid for one polymorph? A myth to dispel, Cryst. Growth Des. 16 (2016) 4582–4588, https://doi.org/10.1021/acs.cgd.6b00682.
[50] L. Gonnet, T.H. Borchers, C.B. Lennox, J. Vainauskas, Y. Teoh, H.M. Titi, C. J. Barrett, S.G. Koenig, K. Nagapudi, T. Friščić, The " η-sweet-spot" (ηmax) in liquid-assisted mechanochemistry: polymorph control and the role of a liquid additive as either a catalyst or an inhibitor in resonant acoustic mixing (RAM), Faraday Discuss 241 (2023) 128–149, https://doi.org/10.1039/D2FD00131D.
[51] M. Arhangelskis, D.-K. Bučar, S. Bordignon, M.R. Chierotti, S.A. Stratford, D. Voinovich, W. Jones, D. Hasa, Mechanochemical reactivity inhibited, prohibited and reversed by liquid additives: examples from crystal-form screens, Chem. Sci. 12 (2021) 3264–3269, https://doi.org/10.1039/D0SC05071G.
[52] D. Hasa, W. Jones, Screening for new pharmaceutical solid forms using mechanochemistry: a practical guide, Adv. Drug Deliv. Rev. 117 (2017) 147–161, https://doi.org/10.1016/j.addr.2017.05.001.
[53] S.N. Madanayake, A. Manipura, R. Thakuria, N.M. Adassooriya, Opportunities and challenges in mechanochemical cocrystallization toward Scaled-Up pharmaceutical manufacturing, Org. Process Res. Dev. 27 (2023) 409–422, https://doi.org/10.1021/acs.oprd.2c00314.
[54] T. Friščić, C. Mottillo, H.M. Titi, Mechanochemistry for synthesis, Angew. Chem. Int. Ed. 59 (2020) 1018–1029, https://doi.org/10.1002/anie.201906755.
[55] S.J. Dengale, H. Grohganz, T. Rades, K. Löbmann, Recent advances in co-amorphous drug formulations, Adv. Drug Deliv. Rev. 100 (2016) 116–125, https://doi.org/10.1016/j.addr.2015.12.009.
[56] D. Zanolla, D. Hasa, M. Arhangelskis, G. Schneider-Rauber, M.R. Chierotti, J. Keiser, D. Voinovich, W. Jones, B. Perissutti, Mechanochemical formation of racemic praziquantel hemihydrate with improved biopharmaceutical properties, Pharmaceutics 12 (2020), https://doi.org/10.3390/pharmaceutics12030289.
[57] D. Zanolla, B. Perissutti, N. Passerini, M.R. Chierotti, D. Hasa, D. Voinovich, L. Gigli, N. Demitri, S. Geremia, J. Keiser, P. Cerreia Vioglio, B. Albertini, A new soluble and bioactive polymorph of praziquantel, Eur. J. Pharm. Biopharm. 127 (2018) 19–28, https://doi.org/10.1016/j.ejpb.2018.01.018.
[58] P. Sanphui, S.S. Kumar, A. Nangia, Pharmaceutical cocrystals of niclosamide, Cryst. Growth Des. 12 (2012) 4588–4599, https://doi.org/10.1021/cg300784v.
[59] B. Bhushan, P. Dubey, S.U. Kumar, A. Sachdev, I. Matai, P. Gopinath, Bionanotherapeutics: niclosamide encapsulated albumin nanoparticles as a novel drug delivery system for cancer therapy, RSC Adv. 5 (2015) 12078–12086, https://doi.org/10.1039/c4ra15233f.
[60] Acetic acid, https://webbook.nist.gov/cgi/cbook.cgi?ID=C64197&Units=SI&Mask=80#IR-Spec (accessed July 16, 2024).
[61] I. D'Abbrunzo, G. Procida, B. Perissutti, Praziquantel fifty years on: a comprehensive overview of its solid state, Pharmaceutics 16 (2023) 27, https://doi.org/10.3390/pharmaceutics16010027.
[62] Y. Xie, Y. Yao, Octenylsuccinate hydroxypropyl phytoglycogen enhances the solubility and in-vitro antitumor efficacy of niclosamide, Int. J. Pharm. 535 (2018) 157–163, https://doi.org/10.1016/j.ijpharm.2017.11.004.
[63] F. Grifasi, M.R. Chierotti, K. Gaglioti, R. Gobetto, L. Maini, D. Braga, E. Dichiarante, M. Curzi, Using salt cocrystals to improve the solubility of niclosamide, Cryst. Growth Des. 15 (2015) 1939–1948, https://doi.org/10.1021/acs.cgd.5b00106.
[64] L. Rosenberger, J. Jenniches, C. von Essen, A. Khutia, C. Kühn, A. Marx, K. Georgi, A.K.H. Hirsch, R.W. Hartmann, L. Badolo, Metabolic profiling of S-praziquantel: structure elucidation using the crystalline sponge method in combination with mass spectrometry and nuclear magnetic resonance, Drug Metab. Dispos. 50 (2022) 320–326, https://doi.org/10.1124/dmd.121.000663.
[65] C. Schlesinger, A. Fitterer, C. Buchsbaum, S. Habermehl, M.R. Chierotti, C. Nervi, M.U. Schmidt, Ambiguous structure determination from powder data: four different structural models of 4,11-difluoroquinacridone with similar X-ray powder patterns, fit to the PDF, SSNMR and DFT-D, IUCrJ 9 (2022) 406–424, https://doi.org/10.1107/S2052252522004237.
[66] A. Wolczyk, B. Paik, T. Sato, C. Nervi, M. Brighi, S.P. GharibDoust, M. Chierotti, M. Matsuo, G. Li, R. Gobetto, T.R. Jensen, R. Černý, S. Orimo, M. Baricco, Li5(BH4)3NH: lithium-rich mixed anion complex hydride, J. Phys. Chem. C 121 (2017) 11069–11075, https://doi.org/10.1021/acs.jpcc.7b00821.
[67] J. van de Streek, M.A. Neumann, Validation of experimental molecular crystal structures with dispersion-corrected density functional theory calculations, Acta Crystallogr. B 66 (2010) 544–558, https://doi.org/10.1107/S0108768110031873.
[68] B. Perissutti, N. Passerini, R. Trastullo, J. Keiser, D. Zanolla, G. Zingone, D. Voinovich, B. Albertini, An explorative analysis of process and formulation variables affecting comilling in a vibrational mill: the case of praziquantel, Int. J. Pharm. 533 (2017) 402–412, https://doi.org/10.1016/j.ijpharm.2017.05.053.
[69] E.C. Van Tonder, T.S.P. Maleka, W. Liebenberg, M. Song, D.E. Wurster, M.M. De Villiers, Preparation and physicochemical properties of niclosamide anhydrate and two monohydrates, Int. J. Pharm. 269 (2004) 417–432, https://doi.org/10.1016/j.ijpharm.2003.09.035.
[70] I. Šagud, D. Zanolla, B. Perissutti, N. Passerini, I. Škorić, Identification of degradation products of praziquantel during the mechanochemical activation, J. Pharm. Biomed. Anal. 159 (2018) 291–295, https://doi.org/10.1016/j.jpba.2018.07.002.
[71] D. Zanolla, B. Perissutti, N. Passerini, S. Invernizzi, D. Voinovich, S. Bertoni, C. Melegari, G. Millotti, B. Albertini, Milling and comilling praziquantel at cryogenic and room temperatures: assessment of the process-induced effects on drug properties, J. Pharm. Biomed. Anal. 153 (2018) 82–89, https://doi.org/10.1016/j.jpba.2018.02.018.
[72] J. Douillet, N. Stevenson, M. Lee, F. Mallet, R. Ward, P. Aspin, D.R. Dennehy, L. Camus, Development of a solvate as an active pharmaceutical ingredient: developability, crystallisation and isolation challenges, J. Cryst. Growth 342 (2012) 2–8, https://doi.org/10.1016/j.jcrysgro.2011.05.023.
[73] C. Zhang, K.M. Kersten, J.W. Kampf, A.J. Matzger, Solid-state insight into the action of a pharmaceutical solvate: structural, thermal, and dissolution analysis of indinavir sulfate ethanolate, J. Pharm. Sci. 107 (2018) 2731–2734, https://doi.org/10.1016/j.xphs.2018.06.020.
[74] Praziquantel EP impurity B | CymitQuimica, https://cymitquimica.com/products/4Z-P-634/125273-86-1/praziquantel-ep-impurity-b/%20(accessed%20on%204%20June%202024). (accessed July 20, 2024).
[75] K. Wang, C.C. Sun, Direct compression tablet formulation of celecoxib enabled with a pharmaceutical solvate, Int. J. Pharm. 596 (2021) 120239, https://doi.org/10.1016/j.ijpharm.2021.120239.
[76] A.M. Tabanez, B.A. Nogueira, A. Milani, M.E.S. Eusébio, J.A. Paixão, H. Nur Kabuk, M. Jajuga, G.O. Ildiz, R. Fausto, Thiabendazole and thiabendazole-formic acid solvate: a computational, crystallographic, spectroscopic and thermal study, Molecules 25 (2020) 3083, https://doi.org/10.3390/molecules25133083.
[77] A. Heinz, C.J. Strachan, K.C. Gordon, T. Rades, Analysis of solid-state transformations of pharmaceutical compounds using vibrational spectroscopy, J. Pharm. Pharmacol. 61 (2009) 971–988, https://doi.org/10.1211/jpp/61.08.0001.
[78] M.D. Eddleston, R. Thakuria, B.J. Aldous, W. Jones, An investigation of the causes of cocrystal dissociation at high humidity, J Pharm Sci 103 (2014) 2859–2864, https://doi.org/10.1002/jps.23865.
[79] M.R. Dhondale, P. Thakor, A.G. Nambiar, M. Singh, A.K. Agrawal, N.R. Shastri, D. Kumar, Co-Crystallization approach to enhance the stability of moisture-sensitive drugs, Pharmaceutics 15 (2023) 189, https://doi.org/10.3390/pharmaceutics15010189.
[80] F.C. Lombardo, B. Perissutti, J. Keiser, Activity and pharmacokinetics of a praziquantel crystalline polymorph in the Schistosoma mansoni mouse model, Eur. J. Pharm. Biopharm. 142 (2019) 240–246, https://doi.org/10.1016/j.ejpb.2019.06.029.